INTERNATIONAL JOURNAL FOR NUMERICAL METHODS IN FLUIDS, VOL. 1, 207–223 (1981)

NUMERICAL SOLUTIONS OF NAVIER–STOKES EQUATIONS WITH AN INTEGRATED COMPARTMENT METHOD (ICM)

GOUR-TSYH YEH

Environmental Sciences Division, Oak Ridge National Laboratory, Oak Ridge, Tennessee 37830, U.S.A.

SUMMARY

The most common numerical methods that are used by physical scientists to approximate partial differential equations employ finite differences and/or finite elements. In addition, compartment analyses have been adopted by ecological system analysts to simulate the evolution of processes governed by differential equations without spatial derivatives. An integrated compartment method (ICM) is proposed to combine the merits of these three numerical techniques. The basic procedures of the ICM are first to discretize the region of interest into compartments, then to apply three integral theorems of vectors to transform the volume integral to the surface integral, and finally to use interpolation to relate the interfacial values in terms of compartment values to close the system. These procedures are applied to the Navier–Stokes equations to yield the computational algorithm from which computer programs can be coded. The computer code is designed to solve one-, two-, or three-dimensional problems as desired. The program is applied to two simple cases: wake formation behind an obstacle in a channel and circulatory motion of a body of fluid in the square cavity. These preliminary applications have shown promising results.

KEY WORDS Numerical Solution Integrated Compartment Method Fluid Dynamics Incompressible Flow

INTRODUCTION

There are many ways in which sets of algebraic equations can be constructed so as to simulate the behaviour of the Navier–Stokes equations, but some methods are more accurate, more convenient to use, or more readily convergent in iterative solution procedures. Since cases for which exact solutions to the Navier–Stokes equations exist are very limited, scientists and engineers are naturally interested in obtaining solutions by numerical means. Thus, rules are needed for the best ways of formulating the corresponding algebraic equations in particular circumstances. Specifically, a solution must be found for a set of elliptic and parabolic differential equations in which both the first and second derivatives of dependent variables appear. This set of equations governs the time-dependent motion of a viscous, incompressible fluid in a region enclosed by very complicated geometries. Therefore, methods to approximate these governing equations and to best represent the region of interest must be continuously developed.

The most common numerical methods used to solve the Navier-Stokes equations are finite differences[1–4] and finite elements.[5–7] The advantages of finite element methods are their inherent ability, because of the integral formulation, to handle complex curved boundaries and their ease in applying natural boundary conditions. Finite difference approximations offer great economy because of simple interpolation for the derivatives. On the other hand,

0271–2091/81/030207–17$01.70

Received August 1980
Revised December 1980

compartment analyses[8] have been widely used by ecological system analysts to simulate the evolution of processes that are governed by differential equations without spatial derivatives. The arbitrary compartmentalization of various shapes and sizes by compartment analyses offers great flexibility of not only discretizing the region but also of more closely representing the compound configurations.

This paper presents a method that combines the merits of the above three categories. The method is termed the integrated compartment method (ICM). It is an extension of the integrated finite difference method—IFDM[9] that was routinely applied to groundwater flow and heat transport problems in the porous media.[10–13] Whereas the IFDM employed only the divergence theorem, ICM will use three integral theorems of vectors. This generalization is necessitated by the fact that the Navier–Stokes equations cannot be carved in terms of only the divergence of some quantities. However, we can easily arrange them in the combinations of gradient, divergence, and curl of the dependent variables.

The basic steps of the ICM are (a) to discretize the region of interest into compartments, (b) to apply three integral theorems of vectors over each compartment to transform the volume integral to the surface integral, and (c) to use simple interpolations to relate the interfacial values in terms of compartment values to close the system. These procedures are applied to the Navier–Stokes equations to yield the computational algorithm from which the computer program is coded. The algorithm is shown to yield conditionally stable and convergent solutions for the pressure and velocity fields. The program is applied to two simple cases for demonstrative purposes. One is the study of the wake behind an obstacle in a channel of finite width; the other is the study of the circulatory motion of a body of fluid in a square cavity.[14] Applications to complex prototype problems will be made in later communications.

INTEGRATED COMPARTMENT METHOD (ICM)

Any numerical method to approximate partial differential equations basically consists of discretization of the region, construction of a set of algebraic equations or coefficient matrices, and solution of the resulting matrix equations. The ICM is thus concerned with discretization, integration, and interpolation. These aspects will be discussed below before they are applied to the Navier–Stokes equations.

Discretization of the region

Fundamental to numerical approaches to solving the Navier–Stokes equations is the concept of discretization, wherein a continuous region is represented as a number of adjacent subregions. While regular-shaped subareas were normally used in the finite difference discretization, irregular-grid finite differences have been developed recently.[15,16] Irregular-shaped grid systems have been routinely employed in the finite element discretization. Practical consideration dictates that a very limited number of shapes (triangular and quadrilateral in two-dimensional cases, or tetrahedron and hexahedron in three-dimensional cases) be used in a particular problem. Besides the difficulty of deriving basis functions for shapes other than these simple ones, programming considerations prohibit the inclusion of a large number of different shapes simultaneously. On the other hand, in compartment analyses, the spatial derivatives do not appear explicitly in the differential equations. The implication is that a compartment or subregion can be any shape and size. The compartment values are, nevertheless, interrelated by the transfer coefficients which represent the interaction between compartments through interfaces. These transfer coefficients are considered as given parameters instead of being obtained by physical principles, resulting in spatial

derivatives. In the proposed ICM method, the implicit feature of the arbitrary division of the system into compartments of different shapes and sizes is retained, but the integral formulation and simple interpolation are applied to the spatial derivatives of the Navier–Stokes equations to obtain the coefficient matrix or the transfer coefficients, so to speak, in the terminology of compartment analyses.

Thus, the first step of the ICM is to divide a continuous region into any number of subregions of various shapes and sizes. Each subregion is termed a compartment. The centroid of a compartment is defined as a node, and the line that connects two nodes is called a connector. The connector is characterized by its two end nodes, the interfacial area, the direction cosine of a unit vector normal to the interface, and the length scales representing the distances from two nodes respectively to the interface. A compartment is characterized by its volume and the nodal number representing it. With these definitions, the region of interest is ready for discretization. For example, Figure 1 shows that the region R is divided into 10 compartments intertwined by 14 interior-to-interior node connectors. For convenience, one may wish to create 11 imaginary boundary compartments and thus 11 interior-to-boundary node connectors in this particular discretization to represent the boundary as in

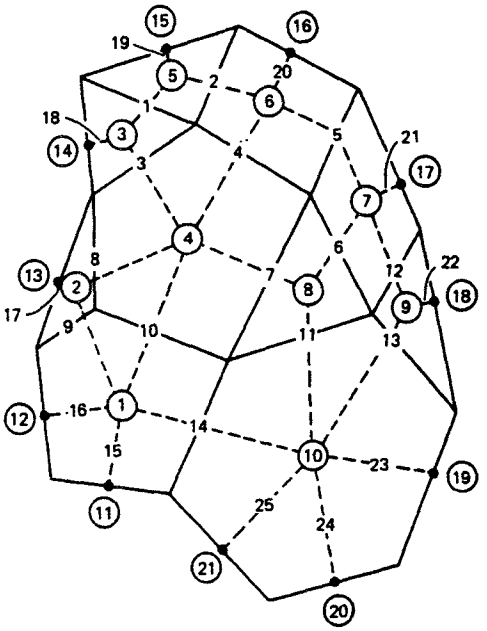

10 INTERIOR COMPARTMENT (NODES): (1) ~ (10)

14 INTERIOR–INTERIOR CONNECTORS (INTERFACES): 1 ~ 14

11 BOUNDARY COMPARTMENT (NODES): (11) ~ (21)

11 INTERIOR–BOUNDARY CONNECTORS (BOUNDARY SEGMENTS): 15 ~ 25

Figure 1. Example of region discretization

Figure 1. The perpendicular distances from boundary compartment nodes to the boundary are set equal to zero. In other words, the boundary nodes are located right on the boundary and the volume of any boundary compartment is zero. Of course, any other subdivision is possible. The major task in employing irregular compartments of various shapes and sizes is, however, the attention and effort demanded for the discretization. Fortunately, methods for automating the discretization of complex regions have been reported elsewhere.[17]

In real applications, discretizing the region cannot be completely arbitrary since instability resulting from grid irregularity can be a problem.[16] Instabilities associated with the irregular compartment discretization are quite like those associated with variable coefficients on uniform compartments. Therefore, for numerical stability, it is important that the sizes and shapes of compartments must be smoothly distributed through the region. In other words, transition of the compartment sizes and shapes from one subregion to another should be gradual in comparison with the coefficients of the differential equations. Properly designed, this should lead to the creation of a well-behaved matrix for the resulting algebraic equations.

Integral formulation

To employ the ICM, the differential equations must first be rearranged and regrouped into combinations of the gradient, divergence, and curl of some quantities. The following integral theorems of vectors are then used to transform the integration of any property over a compartment to that over its interfaces:

$$\int_v \nabla F \, dv = \int_S \mathbf{n} F \, dS \tag{1}$$

$$\int_v \nabla \cdot \mathbf{U} \, dv = \int_S \mathbf{n} \cdot \mathbf{U} \, dS \tag{2}$$

$$\int_v \nabla \times \mathbf{U} \, dv = \int_S \mathbf{n} \times \mathbf{U} \, dS \tag{3}$$

where F and $\mathbf{U}$ are any scalar and vector functions, respectively, dv is the differential volume in the compartment, dS is the differential surface area on the compartment interfaces, and $\mathbf{n}$ is an outward unit vector normal to the enclosing surface. The right-hand sides of equations (1)–(3) can be approximated as follows:

$$\int \mathbf{n} F \, dS \simeq \sum_{j \in N_i} \mathbf{n}_{ij} F_{ij} S_{ij} \tag{4}$$

$$\int \mathbf{n} \cdot \mathbf{U} \, dS \simeq \sum_{j \in N_i} \mathbf{n}_{ij} \cdot \mathbf{U}_{ij} S_{ij} \tag{5}$$

$$\int \mathbf{n} \times \mathbf{U} \, dS \simeq \sum_{j \in N_i} \mathbf{n}_{ij} \times \mathbf{U}_{ij} S_{ij} \tag{6}$$

where the subscript ij indicates that the values are to be evaluated at the interface of compartments i and j as shown in Figure 2, and N_i is the set of compartments surrounding the compartment i. It should be noted that the summation in equations (4)–(6) is to be performed over all the interfaces enclosing compartment i. For example, there are four interfaces, ij, ik, il, and im, surroundings compartment i in Figure 2.

A particularly attractive feature of equations (1)–(6) is their natural consequence of conserving the properties, F and $\mathbf{U}$. For example, equation (5) applied to the continuity

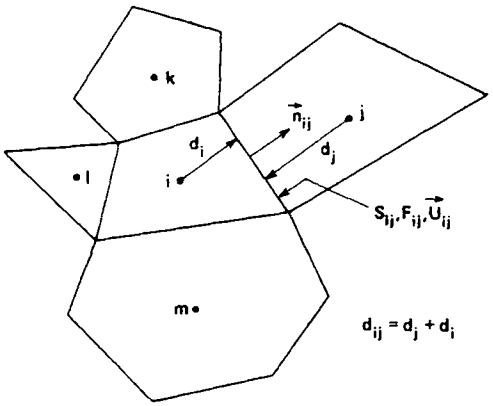

- LINEAR : $F_{ij} = (d_j F_i + d_i F_j)/d_{ij}$
- UPSTREAM : ADVECTION TERM

  $\vec{U}_{ij} \cdot \vec{n}_{ij} \geq 0 \quad \vec{U}_{ij} = \vec{U}_i$

  $\vec{U}_{ij} \cdot \vec{n}_{ij} < 0 \quad \vec{U}_{ij} = \vec{U}_j$
- OTHER : ANALYTICAL LOCAL SOLUTION

Figure 2. Definition of variables and interpolation

equation would guarantee that the mass is conserved numerically. In addition, the novel feature of applying equations (1)–(3) to any spatial derivative is to reduce the problem to the approximation of $(n-1)$th order derivatives on the compartment interfaces rather than the approximation of nth order derivatives at nodal points as used in the irregular-grid finite difference method.[16] This is particularly significant with regard to the first- and second-order derivative terms in the Navier–Stokes equations. Instead of having to approximate both the first- and second-order derivatives by the finite difference methods, one simply has to approximate the function itself and the first-order derivative with simple finite difference interpolation at the interface. Since the first-order derivatives usually define the flux of the property under consideration, the reduction in the order of spatial derivatives makes it simple to build the physical representation at the interfaces, in particular the interface of different media.

Interpolation of interfacial values

Equations (4)–(6) involve the interfacial values. To close the system such that a set of algebraic equations can be obtained in which the number of unknowns equals the number of equations, interpolation methods must be employed to express the interfacial values in terms of the compartment values or the nodal values. The key to the success of the ICM lies in the appropriate interpolations to be used, since they are intimately related to the stability of the numerical solution. There may be infinite varieties of interpolations; the intuitive and simplest is the linear interpolation given by

$$F_{ij} = (d_i F_j + d_j F_i)/(d_i + d_j) \tag{7}$$

where F_i and F_j are the nodal values of compartments, i and j, respectively, and d_i and d_j are the perpendicular distances to the interface, ij, from the nodal points, i and j, respectively, as shown in Figure 2. If the advection terms in the momentum equations are the dominant ones, linear interpolation may lead to an unstable solution so upstream interpolation may be used for such terms:

$$\begin{aligned}(\mathbf{n}_{ij}\cdot\mathbf{U}_{ij})\mathbf{U}_{ij}&=(\mathbf{n}_{ij}\cdot\mathbf{U}_{ij})\mathbf{U}_i \quad \text{if} \quad (\mathbf{n}_{ij}\cdot\mathbf{U}_{ij})>0\\ (\mathbf{n}_{ij}\cdot\mathbf{U}_{ij})\mathbf{U}_{ij}&=(\mathbf{n}_{ii}\cdot\mathbf{U}_{ij})\mathbf{U}_j \quad \text{if} \quad (\mathbf{n}_{ij}\cdot\mathbf{U}_{ij})<0\end{aligned} \tag{8}$$

Another very versatile interpolation is through the analytic solution of a local region. While the linear and upstream interpolations are obvious, the last category requires further explanation. Locally, between nodal points, i and j, the non-linear terms may be linearized, with high probability that analytical solutions may be obtained for the variation of the variable along the connector i–j in terms of its two boundary values.[18] If this is the case, the locally exact solution may be used as the basis for interpolation. Using the exact solution to obtain the interfacial values is naturally superior to any other method. However, it should be noted that exact solutions are seldom obtainable because of the high non-linearity in the Navier–Stokes equations. Nevertheless, this exact interpolation usually is obtainable when one is dealing with the transport of materials having locally constant velocity.

The most serious deficiency that may be encountered in the ICM is that the interpolated value is only a representative value of the interface. The value cannot be identified with a definite point on the interface. This deficiency can be overcome by first interpolating the value of each of the corner points of the interface in terms of the node values whose compartments join at the corner and then interpolating the value at any point on the interface in terms of the values at the corner points. This two-step interpolation procedure would greatly complicate the problem. However, it is worth pursuing for the improvement of the ICM.

ICM APPROXIMATIONS OF THE NAVIER–STOKES EQUATIONS

Governing equations

The starting point for the derivation of the ICM computing algorithm is the vector form of the Navier–Stokes equations for viscous incompressible flow. Since three integral theorems, equations (1)–(3), are used to obtain the ICM approximations, the Navier–Stokes equations are carved in the combinations of these forms as follows:

$$\nabla\cdot\mathbf{U}=0 \tag{9}$$

$$\frac{\partial\mathbf{U}}{\partial t}=-\nabla\Phi-\mathbf{A}+\mathbf{E} \tag{10}$$

$$\Phi=p/\rho+gz \tag{11}$$

$$\mathbf{A}=\nabla\cdot(\mathbf{UU}) \tag{12a}$$

or

$$\mathbf{A}=\nabla(U^2/2)-\mathbf{U}\times\boldsymbol{\omega} \tag{12b}$$

and

$$\mathbf{E}=\nu\nabla^2\mathbf{U} \tag{13a}$$

or

$$\mathbf{E}=-\nu\nabla\times\boldsymbol{\omega} \tag{13b}$$

in which

$$\boldsymbol{\omega} = \nabla \times \mathbf{U} \tag{14}$$

In addition, to facilitate the application of ICM, a divergence quantity is defined by the following equation:

$$D = \nabla \cdot \mathbf{U} \tag{15}$$

In equations (9)–(15), p is the pressure, $\mathbf{U}$ is the velocity vector, ν the kinematic viscosity, ρ the fluid density, g the gravitational acceleration, t the time, z the vertical coordinate, Φ the total potential equal to the pressure and gravitational potentials, $\mathbf{A}$ the advective acceleration, $\mathbf{E}$ is the viscous force, $\boldsymbol{\omega}$ is the vorticity, and D is the divergence of the velocity. These seven equations contain seven unknowns, p, $\mathbf{U}$, Φ, $\mathbf{A}$, $\mathbf{E}$, $\boldsymbol{\omega}$, and D.

It is seen from equations (12a)–(13b) that four alternative forms can be written for the Navier–Stokes equations. These are the combinations of equations (12a) or (12b) and (13a) or (13b). Each form has its advantage from the standpoint of numerical approximations. A thorough discussion is beyond the scope of this paper. Nevertheless, our computer code has provided four options to handle these four alternative forms of the Navier–Stokes equations as described in the following section.

Computational algorithm

The purpose of the ICM procedures is to set up a system of algebraic equations that will approximate the system of equations (9)–(15) for the description of the spatially discrete values $\mathbf{U}_i$, p_i, Φ_i, $\mathbf{A}_i$, $\mathbf{E}_i$, $\boldsymbol{\omega}_i$, and D_i. Thus, applying equations (1)–(6) to equations (12a) or (12b) over the compartment i, one obtains:

$$\mathbf{A}_i v_i = \sum_{j \in N_i} (\mathbf{n}_{ij} \cdot \mathbf{U}_{ij}^{(n)}) \mathbf{U}_{ij}^{(n)} S_{ij} \tag{16a}$$

or

$$\mathbf{A}_i v_i = \sum_{j \in N_i} (\mathbf{n}_{ij} U_{ij}^{2(n)}/2) S_{ij} - \mathbf{U}_i^{(n)} \times \boldsymbol{\omega}_i^{(n)} v_i \tag{16b}$$

where the parenthesized superscript n denotes the value to be evaluated at time $n\Delta t$ and the subscripts i and ij, represent the values of the variable at the compartment, i, and interface, ij, respectively. This convention will be used through the paper. Similarly, applying the ICM method to equations (13a)–(15), one obtains

$$\mathbf{E}_i v_i = \nu \sum_{j \in N_i} (\mathbf{U}_j^{(n)} - \mathbf{U}_i^{(n)}) S_{ij}/d_{ij} \tag{17a}$$

$$\mathbf{E}_i v_i = -\nu \sum_{j \in N_i} \mathbf{n}_{ij} \times \boldsymbol{\omega}_{ij} \tag{17b}$$

$$\boldsymbol{\omega}_i v_i = \sum_{j \in N_i} (\mathbf{n}_{ij} \times \mathbf{U}_{ij}^{(n)}) S_{ij} \tag{18}$$

$$D_i v_i = \sum_{j \in N_i} (\mathbf{n}_{ij} \cdot \mathbf{U}_{ij}^{(n)}) S_{ij} \tag{19}$$

Next, one applies the ICM procedure to the following Poisson equation:

$$\nabla^2 \Phi = D/\Delta t - \nabla \cdot \mathbf{A} + \nabla \cdot \mathbf{E} \tag{20}$$

to yield the discrete total potential at time level, $(n+1)\Delta t$:

$$\sum_{j\in N_i}(\Phi_j^{(n+1)}-\Phi_i^{(n+1)})S_{ij}/d_{ij}=D_i v_i/\Delta t-\sum_{j\in N_i}\mathbf{n}_{ij}\cdot\mathbf{A}_{ij}S_{ij}+\sum_{j\in N_i}(\mathbf{N}_{ij}\cdot\mathbf{E}_{ij})S_{ij} \tag{21}$$

where Δt is the time step. Finally, application of the ICM to equation (10) yields:

$$\mathbf{U}_i^{(n+1)}=\mathbf{U}_i^{(n)}-\Delta t\mathbf{A}_i-\frac{\Delta t}{v_i}\sum_{j\in N_i}\mathbf{n}_{ij}\Phi_{ij}^{(n+1)}S_{ij}+\Delta t\mathbf{E}_i \tag{22}$$

While all interfacial values denoted by the subscript ij in equations (16b) through (19), and (21) and (22) are linearly interpolated in terms of their corresponding connecting nodal values, as given by equation (7), those in equation (16a) are upstreamly interpolated according to equation (8).

It can easily be verified that the new velocity field, $\mathbf{U}^{(n+1)}$, computed by equation (22) satisfies the continuity condition, equation (9). Thus, the $\mathbf{U}$ and Φ fields needed to satisfy the Navier–Stokes equations can be obtained numerically for their discrete fields, $\mathbf{U}_i$ and Φ_i, in space through the time dimension by solving equations (21) and (22). Equations (21) and (22) are two coupled, simultaneous equations. This is true despite the apparent completeness of equation (21) for the solution of the new total potential, $\Phi_i^{(n+1)}$. The reason for this is that the boundary conditions on Φ are expressed in terms of the derivatives of the velocity, $\mathbf{U}_i^{(n+1)}$. However, split techniques have been employed elsewhere[7,19] to solve the finite difference equivalents of equations (21) and (22). It has been indicated that the split technique to decouple the Poisson and momentum equations has yielded a conditionally stable solution.[4,20] Hence, this split procedure is also used to solve equations (21) and (22) separately. In summary, the following procedures are used to advance the solution of $\mathbf{U}$ and p from time level $n\Delta t$ to $(n+1)\Delta t$:

(a) The complete field of the velocity is known at the beginning of the time cycle, either as a result of the previous cycle of calculation or from the prescribed initial conditions. It is assumed that this velocity field is conservative; that is, $D_i^{(n)}$ vanishes everywhere. However, in the real computation, this will never be zero because of roundoff and discretization errors. Hence, a divergence field, $D_i^{(n)}$, is computed by equation (19) and is used as a corrective factor for the Poisson equation.
(b) Advective acceleration, viscous force, and vorticity fields, $\mathbf{A}_i$, $\mathbf{E}_i$, and $\boldsymbol{\omega}_i$, is computed by equations (16a)–(18). This is input into the Poisson equation as the load function.
(c) The new total potential field, $\Phi_i^{(n+1)}$, is obtained by solving equation (21). This may be accomplished by the direct method or a relaxation technique.
(d) The new velocity field, $\mathbf{U}_i^{(n+1)}$, is calculated by equation (22). The new pressure field, $p^{(n+1)}$, is then easily computed by subtracting the gravitational term from the total potential term in equation (11). This completes the advancement of the configuration to the end of the new cycle.

The above time marching procedures are essentially similar to the conventional finite difference method.[1,2,4,9,19–21] The major differences are in the spatial discretization and in the way the spatially discrete fields of pressure and velocity are interrelated. While the applications of conventional finite difference codes such as MAC[19] and SMAC[1] are limited to the regular rectangular grid system, the ICM technique may be applied to any shape and size of discretization. It is seen from equations (16a)–(19) and (21) and (22) that the ICM algorithm is designed in such a way that the change of any quantity in a compartment is equal to the summation of the contributions from all joined connectors and from that within the

compartment itself. As a result of this, the basic algorithm remains the same for cases in one, two, or three dimensions, and it is easy to write a single computer program capable of handling all three classes of problems.

Stability conditions

Since the new velocity is computed explicitly, the time step is limited by the stability conditions. Those conditions have been addressed thoroughly elsewhere.[20] Although they were discussed for finite difference approximations, they are equally valid for the ICM algorithm provided the grid size is interpreted as the compartmental volume divided by the interfacial area. Following the derivations by Hirt,[20] the stability conditions for the cases of expressing the advection in the form of equation (16a) can easily be derived as:

$$\Delta t \leq \frac{2\,\Delta S^2}{4\nu + \dot{U}\,\Delta S} \quad \text{and} \quad \Delta t \leq \frac{2\nu}{U^2} + \frac{\dot{\Delta S}}{\dot{U}} \quad \text{for linear stability} \tag{23}$$

and

$$\Delta S \leq \frac{\dot{U} + (\dot{U}^2 + 8\nu G_U)^{\frac{1}{2}}}{2G_U} \quad \text{for non-linear stability,} \tag{24}$$

where ΔS is the minimum characteristic grid size, U the averaged maximum speed, and G_U the average maximum velocity gradient. It should be pointed out that the terms with dotted circle in equations (23) and (24) are due to the upstream interpolation for the advection given by equation (16a). If linear interpolation had been applied to equation (16a), these terms would disappear.[20] Thus, it is very important that the upstream interpolation must be used if the advection term is expressed in the form of equation (16a). Otherwise both the time step and grid size must be very small such that equations (23) and (24) can be satisfied when the eddy viscosity is very small.

The stability conditions for the cases of expressing the advection in the form of equation (16b) have yet to be derived. I would not expect they would be much different from those in equations (23) and (24). Examination of equation (16b) for the two-dimensional cases reveals an artificial smooth factor. This smooth factor is a direct result of linear interpolation for the kinematic energy and vorticity.

The reason that the same stability conditions hold is obvious, since the time advancement in ICM is practically identical to that in finite differences.[19] The major differences between the ICM and finite difference approximations are in the spatial resolution and in how the spatially discrete values are interrelated.

Boundary conditions

Six types of boundary conditions are considered: no-slip rigid surface, free-slip rigid surface, prescribed normal velocity, prescribed tangential velocity, prescribed pressure, and continuative boundaries. For the no-slip rigid surface, the velocity and total potential at the boundary are computed:

$$u_B = 0, \qquad v_B = 0, \qquad w_B = 0 \tag{25}$$

and

$$\Phi_B = \Phi_I + 2\nu \mathbf{n} \cdot \mathbf{U}_I / d_{IB} \tag{26}$$

where the subscript B denotes the values at the boundary, the subscript I represents the value at the compartment I that has one of its sides coinciding with the boundary, $\mathbf{n}$ is a unit

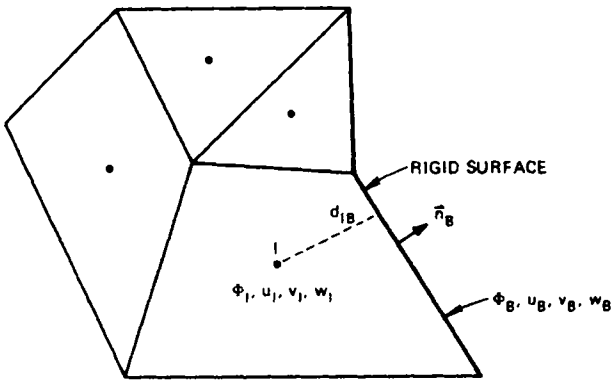

Figure 3. Definition of boundary variables

vector normal outwardly to the fluid (i.e. inwardly to the rigid surface), and d_{IB} is the perpendicular distance from node I to the boundary as shown in Figure 3.

For the free-slip rigid surface, equation (26) without the second term on the right-hand side is used to compute Φ_B, but the following equations are used to obtain the boundary velocity components:

$$u_B = u_I - n_x(\mathbf{n} \cdot \mathbf{U}_I) \tag{27a}$$

$$v_B = v_I - n_y(\mathbf{n} \cdot \mathbf{U}_I) \tag{27b}$$

$$w_B = w_I - n_z(\mathbf{n} \cdot \mathbf{U}_I) \tag{27c}$$

Equation (25) is derived based on the requirements that both the normal and tangential velocities on the surface are zero, whereas the requirements of equation (27) are to satisfy the conditions of vanishing normal velocity at the boundary and equalling the tangential velocities at the boundary and its corresponding interior node. Equation (26) is consistent with the vanishing of the normal velocity at the boundary. The prescribed normal velocity, tangential velocity, and pressure conditions are obvious to implement, and the continuative boundary simply allows the fluid to pass out of the region at its own chosen rate.

For the case of the prescribed normal velocity condition, it will be presumed that the tangential velocity is zero, and for the prescribed tangential velocity condition, that the normal velocity is zero. Under these assumptions, the following equations are used to compute the velocity and Φ at the prescribed normal velocity boundary:

$$u_B = n_x(\mathbf{n} \cdot \mathbf{U}_n), \qquad v_B = n_y(\mathbf{n} \cdot \mathbf{U}_n), \qquad w_B = n_z(\mathbf{n} \cdot \mathbf{U}_n) \tag{28}$$

$$\Phi_B = \Phi_I + 2\nu[(\mathbf{n} \cdot \mathbf{U}_n) - (\mathbf{n} \cdot \mathbf{U}_I)]/d_{IB} \tag{29}$$

where $\mathbf{U}_n$ is the prescribed normal velocity vector. On the prescribed tangential velocity boundary with $\mathbf{U}_t$, the following equations are used:

$$u_B = u_t - n_x(\mathbf{n} \cdot \mathbf{U}_t) \tag{30a}$$

$$v_B = v_t - n_y(\mathbf{n} \cdot \mathbf{U}_t) \tag{30b}$$

$$w_B = w_t - n_z(\mathbf{n} \cdot \mathbf{U}_t) \tag{30c}$$

$$\Phi_B = \Phi_I - 2\nu(\mathbf{n} \cdot \mathbf{U}_I)/d_{IB} \tag{31}$$

where u_t, v_t, and w_t are the x-, y-, and z-components, respectively, of $\mathbf{U}_t$.

For the prescribed pressure boundary with known Φ_p, the following two equations are used:

$$u_B = u_I, \qquad v_B = v_I, \qquad w_B = w_I \tag{32}$$

$$\Phi_B = \Phi_p \tag{33}$$

Finally, for the continuative boundary, the following equations may be used:

$$U_B = u_I, \qquad v_B = v_I, \qquad w_B = w_I, \qquad \Phi_B = gz_B \tag{34}$$

Boundary conditions for Φ_B in equations (26), (29), and (31) are, in fact, obtained by applying equation (10) to the boundary compartment and incorporating the corresponding conditions for the velocity vector, **U**, whereas in equations (33) and (34), Φ_B is determined by assuming that the pressure is given.

SAMPLE CALCULATIONS

Two calculational examples are used to illustrate the behaviour of the Navier–Stokes equations as simulated by the ICM algorithm. One is the study of the wake behind an obstacle in a channel of finite width, while the other is the circulatory motion of a body of fluid in a square cavity. Although the computer program has been designed for handling two- and three-dimensional problems as desired, it is applied to these simple two-dimensional cases for illustrative purposes. In addition, the study of the wake is a prerequisite for investigating vortex shedding and computing the drag forces on the obstacle, and the cavity problem has relevance in bearing and seal studies.

In the first example, the fluid is assumed initially at rest in a channel with an infinitely long rectangular prism located in the centre between the walls whose spacing is 90 cm. The total length of the channel included for the computation is artificially terminated at 130 cm. The obstacle is located 40 cm from the channel entrance. The width and length of the obstacle are both assumed to be 10 cm. For the ICM simulation, the channel is divided into a 13×9 square mesh resulting in 116 fluid compartments and one obstacle compartment, each with a size of 10×10 cm. The walls of the channel are considered to be no-slip rigid surfaces as is the obstacle. The channel entrance is considered as the prescribed normal-flow boundary and the exit is treated as the continuative boundary. The eddy viscosity is taken as $0{\cdot}01\ \mathrm{cm^2\ s^{-1}}$, a representative value for water at 20°C. The computation starts at $t = 0$ s with the fluid at the entrance impulsively accelerated to the velocity of $1{\cdot}0\ \mathrm{cm\ s^{-1}}$ and maintained at this velocity throughout the calculation. Figure 4 shows the flow pattern after $t = 720$ s when it can be thought of as having reached the steady state. The prominent feature of a long, slender, eddy vortex just behind the obstacle is clearly observed.[22] Each vortex produces a back-flow (note arrow direction in Figure 4) over the rear portion of the obstacle. This symmetrical pair is, however, very susceptible to antisymmetrical disturbances[21] because it provides the main mechanism for vortex shedding.

To investigate the effect of the obstacle size on the wake formation, the width of the obstacle is tripled and the simulation is repeated. The resulting flow pattern is shown in Figure 5. It is seen that the length of the vortex behind the obstacle is even greater. The reverse flow in the wake extends to the continuative boundary. This means that a portion of fluid is redrawn into the region of interest after it leaves the continuative boundary.

Careful examination of this simple example indicates an interesting phenomenon that needs further elaboration. It has been pointed out that for the Reynolds number, $Re = u_0 d/\nu$ (where u_0 is the free stream fluid speed, d is the height of the obstacle, and ν is the

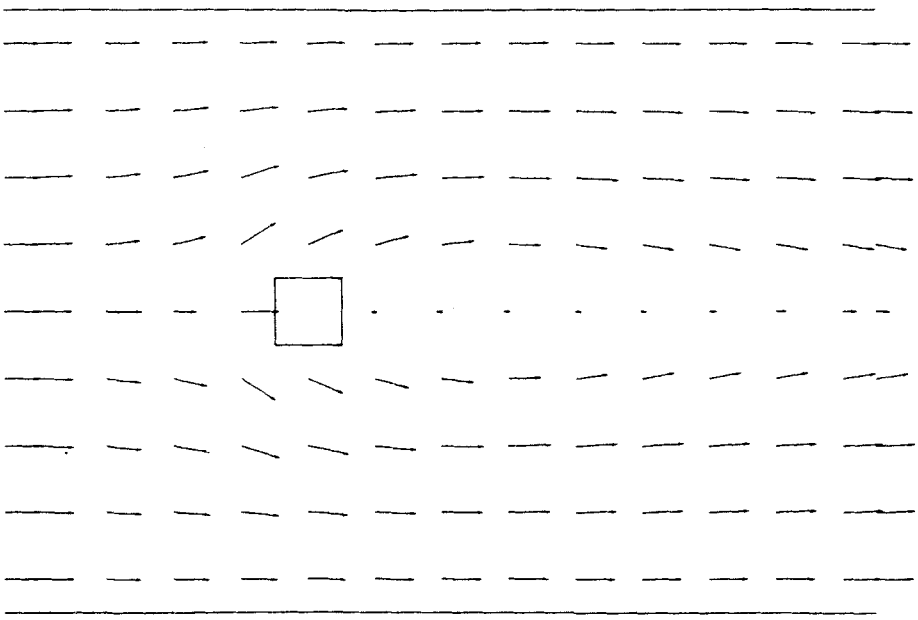

Figure 4. Velocity plot of wake behind a small obstacle in a channel at time = 720 s

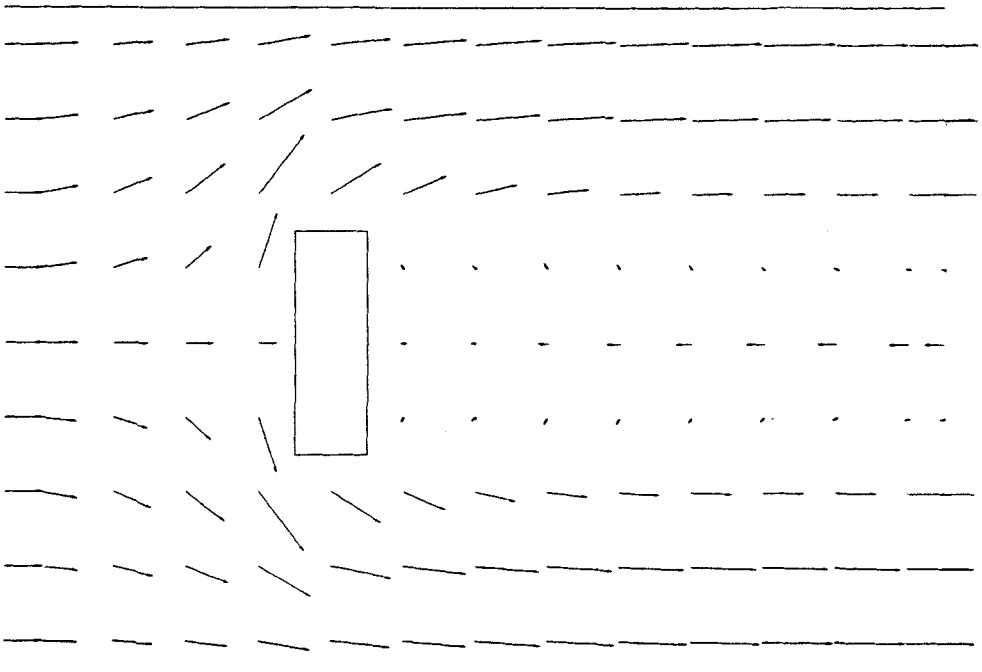

Figure 5. Velocity plot of wake behind a large obstacle in a channel at time = 720 s

kinematic viscosity), greater than 50, the steady flow is unstable and vortices are shed.[21] In other words, the vortices should not be 'regular' for *Re* greater than 50 and the effect of turbulence should become more and more pronounced as Reynolds number, *Re*, increases. In the case of a small obstacle in this example, the Reynolds number is 1000, while for the case of a big obstacle, it is 3000. For such high Reynolds numbers, the stable steady-state solutions should not persist or even probably exist. These puzzling situations are surmised to result from the geometrical symmetry and numerical viscosity on coarse computational grid systems. Since the solution procedures preserve symmetry to more than six digits, the steady solution often persists for long periods of time, even for large values of the Reynolds number. Thus, to effectively start the vortex shedding process, a necessary condition is to introduce an artificial antisymmetric mechanism in the computation. In fact, an artificial perturbation of vortices can be created in front of the obstacle to destroy the symmetry and to start the vortex shedding[21] within a fairly short time. The destruction of symmetry provides requisite conditions for shedding. A seemingly important factor, however, that causes resistance to shedding is the numerical viscosity that results from coarse grid systems in conjunction with upstream interpolation.

It is easy to show that upstream interpolation will yield an effective numerical viscosity, ν_N, as defined by the following equation:[23]

$$\nu_N = \tfrac{1}{2}u(1 - u\Delta t/\Delta s)\,\Delta s \tag{35}$$

Taking the values for $u = 1\ \text{cm s}^{-1}$, $\Delta s = 10$ cm, and $\Delta t = 1{\cdot}5$ s (the time-step size used for this sample problem), equation (35) gives ν_N equal to $4{\cdot}25\ \text{cm}^2\ \text{s}^{-1}$, resulting in a numerical Reynolds number of 2·35. Thus, to *start* the vortex shedding process, a fine grid of smaller than $\Delta s = 1{\cdot}9$ cm for the case of small obstacle or $\Delta s = 2{\cdot}7$ cm for the case of big obstacle would probably be required in addition to an antisymmetric mechanism. This computation is based on the assumption that the instability of the vortex will eventually occur for Reynolds numbers greater than 50.[21] The higher the Reynolds number, the greater the length of the eddy region will usually be. The onset of vortex shedding thus depends on the Reynolds number since the mechanism for it depends on the lengthening of the steady state vortex.[21,22] It is, however, beyond the scope of this paper to devise antisymmetric perturbations for investigating the onset of vortex shedding processes and the vortex street phenomena[21] with finer grid meshes.

As a second example to illustrate the application of the ICM, fluid initially at rest in a square cavity is set into circulatory motion within the cavity by a boundary moving in its own plane at the top. The calculation is characterized by a Reynolds number shich is $LU_w/\nu = 100$, where L and U_w are the constant length and velocity of the top wall. This Reynolds number is chosen because cavity flow with this number has been investigated experimentally and numerically[14,24,25] so that comparison with prior work is possible. Time-exposure photographs have been taken[24,25] of flows into which a tracer has been injected so that the qualitative features of the steady flow are known.[14]

To start the ICM computation, the cavity is divided into 100 compartments, each 10×10 cm. The constant moving velocity on the top wall is taken to be $1{\cdot}0\ \text{cm s}^{-1}$, and the viscosity is chosen to be $1{\cdot}0\ \text{cm}^2\ \text{s}^{-1}$ to make the Reynolds number 100. The flow pattern at time equal to 1440 s when it has reached steady state is shown in Figure 6. Comparison of this flow configuration with the time exposure photograph of steady flow reported by Mills[24] and reproduced by Donovan[14] shows almost identical qualitative results. The vortex centre in Figure 6 is about 76 cm from the bottom and 62 cm from the left wall. This vortex centre

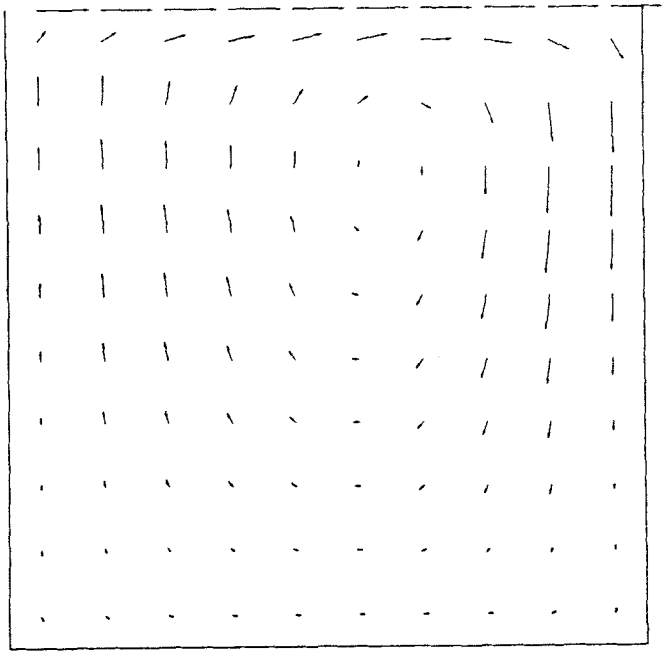

Figure 6. Velocity plot of circulation in the square cavity with large grid discretization at time = 1440 s

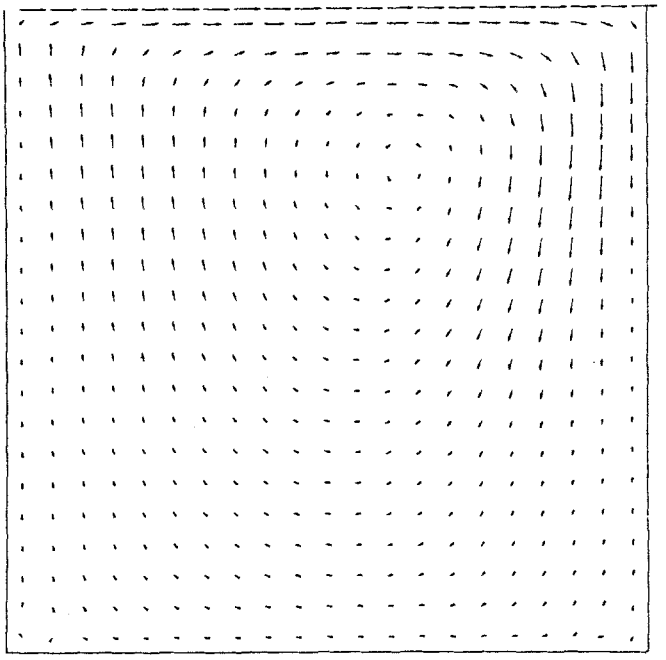

Figure 7. Velocity plot of circulation in the square cavity with small grid discretization at time = 1440 s

is in nearly perfect agreement with the experimental vortex centre determined by Donovan[14] from the enlargement of the photograph by Mills.[24]

To test the effects of compartment size on the computation, the same cavity is divided into 441 square compartments, and the calculation is repeated by the ICM computer program. The resulting flow is shown in Figure 7. The vortex centre is 'almost identical' to that in Figure 6. The velocity fields as computed by two spatial discretizations with different compartment sizes show no appreciable differences. However, while all fluid rotates about the vortex centre in Figure 6, two small counterrotating vortices exist in the two lower corners in Figure 7, although the main vortex occupies most of the cavity. It is thus seen that as the compartment size becomes smaller, smaller-scale vortices can be found.[25] Interestingly, Moffatt[26] also found these smaller vortices at about the same location using analytical techniques for the boundary-layer region.

Figures 4–7 illustrate only the qualitative trend of flow visualization. It is instructive at this point to compare our numerical results with those obtained by Mills[24] and Donovan[14] for the quantitative assessment of the ICM procedure. The position of the vortex centre and the patterns of the circulation in the cavity problem have yielded excellent agreement with previously published results.[14,24,25] Another definite aspect of agreement is illustrated in Figure 8, which shows the distribution of x-component velocities along a line perpendicular to the moving surface and passing through the centre of the vortex. It shows excellent agreement with those reported by Mills[24] and acceptable comparison with those by Donovan.[14] The distribution of y-component velocity along a line parallel to the moving surface and passing through the vortex centre is shown in Figure 9. Nearly identical agreement with Donovan[14] is obtained and acceptable agreement with Mills[24] is achieved.

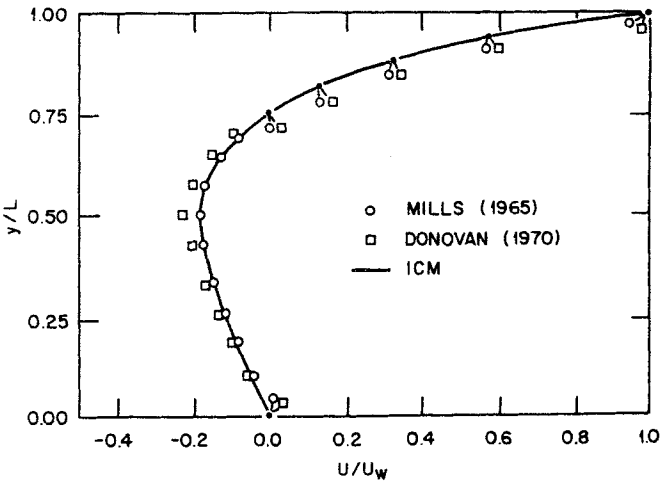

Figure 8. Comparison of x-component velocity distribution as simulated by Mills, Donovan, and the ICM along a line perpendicular to the moving surface as passing through the vortex centre.

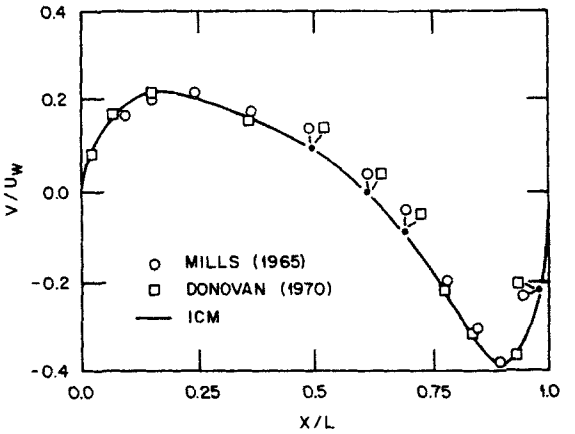

Figure 9. Comparison of y-component velocity distribution as simulated by Mills, Donovan, and the ICM along a line parallel to the moving surface and passing through the vortex centre.

CONCLUSION

A technique, an integrated compartment method (ICM), has been developed to set up the algebraic equations from the Navier–Stokes equations. It uniquely combines the merits of finite differences, finite elements, and compartment analyses. The time-split procedure proposed by several investigators to advance the pressure and velocity fields through the time dimension is adopted to accomplish the evolution of flow dynamics by the ICM algorithm. The computer code designed to handle two- and three-dimensional problems as desired is made to implement this technique. The program is applied to two simple cases of wake formation behind the obstacle in a channel and circulatory motion of a body of fluid in the square cavity. The preliminary application has shown promising results. Adoption of the program to study general three-dimensional fluid problems in complex regions is open for further investigation.

ACKNOWLEDGMENT

This research is supported in part by the Office of Nuclear Waste Management, U.S. Department of Energy, under contract W-7405-eng-26, and in part by the Office of Toxic Substances, U.S. Environmental Protection Agency, with Union Carbide Corporation. Publication No. 1727, Environmental Sciences Division, Oak Ridge National Laboratory.

REFERENCES

1. A. A. Amsden and F. H. Harlow, *The SMAC: A Numerical Technique for Calculating Incompressible Fluid Flows*, LA-4370, Los Alamos Scientific Laboratory, Los Alamos, New Mexico, 1970.
2. A. J. Chorin, 'A numerical method for solving incompressible viscous flow problems', *J. Comput. Phys.*, **2**, 12–26 (1967).
3. G. E. Forsythe and W. R. Wasow, *Finite-Difference Methods for Partial Differential Equations*, Wiley, New York, 1960.
4. F. H. Harlow and J. E. Welch, 'Numerical calculation of time dependent viscous incompressible flow of fluid with free surface', *Phys. Fluids*, **8**, 2182–2189 (1965).
5. S. L. Smith and C. A. Brebbia, 'Finite element solution of Navier–Stokes equations for transient two-dimensional incompressible flow', *J. Comput. Phys.*, **17**, 235–245 (1975).

6. C. Taylor and P. Hood, 'A numerical solution of the Navier–Stokes equations using the finite element technique', *Comput. Fluids*, **1**, 73–100 (1973).
7. O. C. Zienkienwicz, *The Finite Element Method*, 3rd edn, McGraw-Hill, New York, 1977.
8. J. A. Jacquez, *Compartmental Analysis in Biology and Medicine*, Elsevier, New York, 1972.
9. T. N. Narasimhan and P. A. Witherspoon, 'An integrated finite difference method for analyzing fluid flow in porous media', *Water Resour. Res.*, **12**, 57–67 (1976).
10. A. L. Edwards, 'TRUMP: a computer program for transient and steady-state temperature distributions in multidimensional systems', *UCRL-14754, Rev.* 3, Lawrence Livermore Laboratory, Livermore, California, 1972.
11. M. J. Lippmann, C. F. Tsang, and P. A. Witherspoon, 'Analysis of the response of geothermal reservoirs under injection and production procedures', *Proc. 47th Annual California Regional Meeting of the Society of Petroleum Engineers of AIME*, Berkeley, California, 1977, pp. 1–15.
12. T N. Narasimhan, P. A. Witherspoon, and A. L. Edwards, 'Numerical model for saturated–unsaturated flow in deformable porous media 2. The algorithm', *Water Resour. Res.*, **14**, 255–261, 1977.
13. T. N. Narasimhan and W. A. Palen, 'A purely numerical approach for analyzing flow to a well intercepting a vertical fracture', *LBL-8816*, Lawrence Berkeley Laboratory, Berkeley, California, 1979.
14. L. F. Donovan, 'A numerical solution of unsteady flow in a two-dimensional square cavity', *J. AIAA*, **8**, 524–529 (1970).
15. J. P. Boris, K. L. Hain, and M. J. Fritts, 'Free surface hydrodynamics using Lagrangian triangular mesh', *Proc. First International Conference on Numerical Ship Hydrodynamics*, 20–23 October 1975, David W. Taylor Naval Ship Research and Development Center, 1975.
16. W. C. Thacker, 'Irregular grid finite-difference technique: simulation of oscillations in shallow circular basins', *J. Phys. Oceanogr.*, **7**, 284–292 (1977).
17. W. C. Thacker, A. Gonzaleg, and G. E. Putland, 'A method for automating the construction of irregular computational grids for storm surge forecast models', *J. Comp. Phys.*, (1980) (in press).
18. D. B. Spalding, 'A novel finite difference formulation for differential equations involving both first and second derivatives', *Int. J. num. methods Engng.*, **4**, 551–559 (1972).
19. J. E. Welch, F. H. Harlow, J. P. Shannon, and B. J. Daley, *The MAC Method: A Computing Technique for Solving Viscous Incompressible Transient Fluid Flow Problems Involving Free Surfaces*, LA-3745, Los Alamos Scientific Laboratory, Los Alamos, New Mexico, 1966.
20. C. W. Hirt, 'Heuristic stability theory for finite difference equations', *J. Comput. Phys.*, **2**, 339–355 (1968).
21. J. E. Fromm and F. H. Harlow, 'Numerical solution of vortex street development', *Phys. Fluids*, **6**, 975–982 (1963).
22. S. Goldstein, *Modern Developments in Fluid Dynamics*, Dover, New York, 1965.
23. C. R. Molenkamp, 'Accuracy of finite-difference methods applied to the advection equation, *J. Appl. Meteorol.*, **7**, 160–167 (1968).
24. R. D. Mills, 'Numerical solution of the viscous flow equation for a class of closed flows', *J. R. Aeronaut. Soc.*, **69**, 714–718 (1965).
25. C. F. Pan and A. Acrivos, 'Steady flow in rectangular cavities', *J. Fluid Mech.*, **28**, 643–655 (1967).
26. H. K. Moffatt, 'Viscous and resistive eddy near a shape corner', *J. Fluid Mech.*, **18**, 1–15 (1964).